MethodsX 11 (2023) 102475

Contents lists available at ScienceDirect

MethodsX

journal homepage: www.elsevier.com/locate/methodsx

A spectrum-of-spectrum filtering method to extract direct and multipath arrivals from simulations and measurements

Eivind Nag Mosland[a,*], Per Lunde[a], Jan Kocbach[b]

[a] Department of Physics and Technology, University of Bergen, P.O. Box 7803, Bergen N-5020, Norway
[b] NORCE Norwegian Research Centre AS, P.O. Box 22 Nygårdstangen, Bergen N-5838, Norway

ARTICLE INFO

Method name:
Spectrum-of-spectrum filtering

Keywords:
Echo removal
Multipath removal
Fourier transform
Acoustic simulation
Acoustic measurements
Signal processing
Ultrasound
SoS filtering
Cepstrum
Cepstral

ABSTRACT

In measurements and numerical modelling of wave propagation, undesired interference between direct and multipath arrivals can be reduced using Fourier-based signal processing methods. Existing methods, such as cepstral analysis and time-signal gating, are not applicable to all cases. Here, an alternative Fourier-based signal processing method is presented, called spectrum-of-spectrum (SoS) filtering. Its main advantage over existing methods is its ability to extract single direct or multipath arrivals for relatively short propagation distances even when subsequent arrivals do not become successively weaker. The method is based on the following steps:

- Apply a lowpass filter to the real and imaginary parts of an input frequency spectrum individually, using a digital finite impulse response (FIR) filter in the frequency domain.
- Recombine the filtered real and imaginary parts of the frequency spectrum to get the frequency spectrum of the direct arrival.
- For extraction of the first multipath arrival, subtract the filtered frequency spectrum from the input frequency spectrum and repeat the previous steps. Repeat multiple times to extract subsequent multipath arrivals.

Specifications table

Subject area:	Physics and Astronomy
More specific subject area:	Signal processing
Name of your method:	Spectrum-of-spectrum filtering
Name and reference of original method:	N.A.
Resource availability:	N.A.

Method details

Multipath arrivals can interfere with the direct arrival in measurements and in numerical simulations, for instance in acoustics and electromagnetics, and can be seen as oscillations or periodicity in the frequency spectrum. Different signal processing methods have been applied for multipath removal, for instance cepstral (e.g., [1]) and time-signal gating [2] methods.

Cepstral methods are based on calculating the forward or inverse Fourier transform of the natural logarithm of the frequency spectrum, yielding its cepstrum [1,3], and combining this with filtering or more advanced methods [1,4] to remove undesired multipath

* Corresponding author.
E-mail address: eivind.mosland@uib.no (E.N. Mosland).

https://doi.org/10.1016/j.mex.2023.102475
Received 8 June 2023; Accepted 4 November 2023
Available online 7 November 2023

arrivals, e.g., echoes. Using the natural logarithm of the spectrum increases the perceived "relative strength of weaker echoes" [4], which may be beneficial for the subsequent analysis and processing. However, it may also be unnecessary or have adverse effects [4–6]. For the special case where the magnitudes of interfering multipath arrivals do not decrease compared to the direct arrival, cepstral filtering will likely yield erroneous results, as shown in [7].

Time-signal gating makes use of Fourier synthesis to generate a train of tone bursts corresponding to the direct arrival and the subsequent multipath arrivals [2]. By use of time gating, the time-signal corresponding to the desired arrival may be extracted and its frequency spectrum calculated. A necessary condition for it to work is that steady-state conditions are achieved in the tone bursts prior to the subsequent arrival. Time-signal gating is typically used for multipath removal or extraction in frequency domain transfer functions derived from numerical simulations were harmonic time dependence (continuous waves) is assumed [2,7]. It may be used for the special case described above, but generally yields poor results at short distances and for narrowband transducers, for which steady-state conditions may not be not achieved [7].

An alternative method is presented here, denoted spectrum-of-spectrum (SoS) filtering, which has improved performance compared to the cepstral and time-signal gating methods for the special case where the magnitude of interfering multipath arrivals does not decrease [7]. SoS filtering of the frequency spectrum can be used to extract the direct arrival or any multipath arrival, and can be applied to, e.g., acoustic, electroacoustic, or electromagnetic problems. SoS filtering is somewhat similar to cepstral filtering in design, but (i) omits the natural logarithm and other types of "spectral whitening" [6], and (ii) the Fourier transforms and filtering are calculated individually for the real and imaginary parts of the frequency spectrum. The method is based on lowpass filtering of the real and imaginary parts of the frequency spectrum, using a digital finite impulse response (FIR) filter. The filter is designed based on the SoS, which is here defined as the forward Fourier transform of the frequency spectrum, calculated individually for the real and imaginary parts.

The main steps of SoS filtering of the frequency spectrum for extraction of the direct arrival are:

1. Obtain the input frequency spectrum, $X(f)$, which includes both direct and multipath arrivals.
2. Design a linear-phase digital FIR lowpass filter, based on an analysis of the SoS, to retain as much as possible of the information associated with the direct arrival, while removing as much as possible of the information associated with the multipath arrivals.
3. Perform individual lowpass filtering of the real and imaginary parts of $X(f)$ using the FIR filter from step 2 to calculate the real and imaginary parts of the filtered frequency spectrum, $X_1(f)$, i.e., the parts of $X(f)$ primarily containing information about the direct arrival. The filtering is applied in the frequency domain.
4. Recombine the real and imaginary parts of $X_1(f)$.

To extract the first multipath arrival, $X_2(f)$, first obtain $X_1(f)$ using steps 1–4 above, and then repeat steps 1–4 with $X(f) - X_1(f)$ as the input frequency spectrum, and adjusted filter settings in step 2. This process can be repeated multiple times to yield the higher order multipath arrivals, $X_n(f)$, $n = \{3, 4, \ldots\}$. An alternative to this successive process is to apply a bandpass filter to $X(f)$ in step 3 to keep the information associated with a specific arrival and remove the rest.

If the frequency spectrum $X(f)$ contains rapid changes with a rate of change as large or larger than the oscillations caused by multipath interference, e.g., sharp resonance peaks, this will negatively impact the SoS filtering around these rapid changes. However, results can be improved by application-specific preprocessing prior to SoS filtering, i.e., that a preprocessing is applied to $X(f)$ to yield a preprocessed frequency spectrum $X^p(L, f)$, and this $X^p(L, f)$ is SoS filtered instead of $X(L, f)$. The SoS filtering will then yield $X_1^p(L, f)$, which must be postprocessed by reversing the preprocessing to yield $X_1(L, f)$.

A harmonic time dependence of $e^{i\omega t}$ is assumed in the examples presented here, where $i = \sqrt{-1}$, $\omega = 2\pi f$ is the angular frequency, t is time, and the forward Fourier transform of a time waveform $X(t)$ is defined as

$$X(f) = \int_{-\infty}^{\infty} X(t) e^{-i2\pi f t} dt \ . \tag{1}$$

The forward Fourier transform is needed to design the FIR filter, but the corresponding inverse Fourier transform is not needed since the SoS filtering is performed by applying the digital filter to the frequency spectrum. The spectrum of the spectrum of the real and imaginary parts of $X(f)$ are calculated by treating them as waveforms and applying the forward Fourier transform, i.e.,

$$\mathcal{F}[\mathrm{Re}(X(f))] = \int_{-\infty}^{\infty} \mathrm{Re}(X(f)) e^{-i2\pi f t} df, \tag{2}$$

and

$$\mathcal{F}[\mathrm{Im}(X(f))] = \int_{-\infty}^{\infty} \mathrm{Im}(X(f)) e^{-i2\pi f t} df, \tag{3}$$

respectively.

The real and imaginary parts of the input frequency spectrum $X(f)$ are treated separately for ease of interpretation and implementation. $\mathrm{Re}(X(f))$ and $\mathrm{Im}(X(f))$ can be filtered using a regular digital filter since both are real numbers. Their forward Fourier transforms, i.e., SoSs, are symmetric, which simplifies the analyses. If a time convention $e^{-i\omega t}$ is used instead of $e^{i\omega t}$, the SoS method is identical to the one described here, but with "i" instead of "$-i$" in all expressions and calculations.

MATLAB® code implementing SoS filtering of the frequency spectrum, used to extract the direct arrival and first multipath arrival for a plane wave example, is included in Figs. 12 and 13. The code utilizes the *lowpass* function, which is included in the Signal Processing Toolbox™ [8], but is otherwise self-contained and does not rely on external datasets.

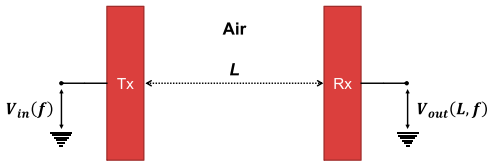

Fig. 1. Schematic of modelled ultrasonic transmit-receive measurement system with a transmitting cylindrical piezoelectric transducer (Tx) and a receiving cylindrical transducer (Rx) at the axial distance L, both freely suspended in air and coaxially aligned. 3D axial symmetry is assumed around the axis passing through the center of both transducers.

Example without application-specific preprocessing

The method is presented in more detail for an example case of a frequency domain numerical simulation of an acoustic transit-receive measurement system where SoS filtering of the frequency spectrum is used to find the voltage-to-voltage transfer function for the direct arrival. A 3D axisymmetric finite element (FE) model is used to calculate the voltage-to-voltage transfer function between two identical coaxially aligned piezoelectric cylindrical disks acting as ultrasonic transducers. A schematic of the example case is shown in Fig. 1. The transducers are freely suspended in an unbounded medium, air, at a distance $L = 0.20$ m apart. The air is assumed to be lossless and is modelled with a sound velocity of $c = 343$ m/s. Modelling details are found in [7,9]. The voltage-to-voltage transfer function from the transmitter to the receiver is defined as

$$H^{VV}(L,f) = \frac{V_{out}(L,f)}{V_{in}(f)}, \tag{4}$$

where $V_{in}(f)$ is the excitation voltage at the transmitter and $V_{out}(L,f)$ is the open-circuit output voltage at the receiver at the distance L and frequency f. The frequency range 50–200 kHz is considered, with a frequency resolution of 0.1 kHz.

Due to the monoharmonic continuous wave excitation in the frequency domain simulation, the output voltage at the receiver is the sum of the direct arrival and multipath arrivals caused by reflections at the transducers, yielding standing waves between the transducers. For a given distance L, the phase delays between the arrivals vary as a function of frequency, causing alternating constructive and destructive interference and thus oscillations in the frequency spectrum of $H^{VV}(L,f)$. This is deemed to be the main cause of the oscillations in $H^{VV}(L,f)$ for the presented example.

An additional contributor to the oscillation in the frequency spectrum is the varying coupling between the transducers and medium as the frequency changes, caused by the standing waves. At transmission, this can be interpreted as a change in the radiation impedance and can be observed as oscillations in the electrical input impedance of the system. Since such standing waves will generally not occur in measurements using tone bursts, their effects should ideally be accounted for when extracting results for a single arrival. An analysis of the oscillations in the electrical input impedance shows comparable oscillation characteristics in the SoS as for the $H^{VV}(L,f)$. This indicates that the effects of the varying coupling may be accounted for by the SoS filtering method, although further studies are needed to confirm this. Furthermore, it is likely that such coupling effects are more important in denser fluids, such as liquids, than for the current example in air.

Step 1: The frequency spectrum considered as input to the SoS filtering is

$$X(L,f) = H^{VV}(L,f), \tag{5}$$

for $L = 0.20$ m. The magnitude and phase angle of $X(L,f)$ are shown in Fig. 2, and the corresponding real and imaginary parts are shown in Fig. 3. The slowly varying phase of $X(L,f)$ is also shown in Fig. 2c to better visualize the oscillations in phase angle, obtained by dividing $X(L,f)$ by the phase term for the plane wave transit time of the direct arrival, $e^{-i\omega L/c}$. The oscillations in the magnitude and slowly varying phase of $X(L,f)$ are caused by the interfering multipath arrivals.

To avoid visually misleading plots of the phase angles in Figs. 2, 7, 10, and 11 due to phase wrapping and a relatively sparse frequency resolution, the frequency step size has—for the plotting only—been reduced using linear interpolation of the unwrapped phase angles of $X(L,f)$, $X(L,f)/e^{-i\omega L/c}$, $X_1(L,f)$, and $X_1(L,f)/e^{-i\omega L/c}$. In Figs. 2 and 7 the frequency step size is reduced from 0.1 kHz to 0.01 kHz and in Figs. 10 and 11 it is reduced from 0.1 kHz to 0.001 kHz.

Steps 2 and 3: A lowpass filter is applied to the real and imaginary parts of $X(L,f)$ to keep as much as possible of the information related to the direct arrival and remove as much as possible of the information related to the multipath arrivals. This digital filter is applied in the frequency domain, specified to impact the spectrum of the spectrum. Thus, the filter design is based on analysis of the spectrum of the spectrum of $X(L,f)$ shown in Fig. 4. The SoS is a function of time, although it is distinctly different from the impulse response corresponding to $X(L,f) = H^{VV}(L,f)$. There are distinct features starting at approximately 0.6, 1.8, and 2.9 ms, approximately equal to

$$(2n-1)L/c, \tag{6}$$

for $n = \{1,\ 2,\ 3\}$, respectively. The first feature, A, contains information regarding the direct arrival, while the subsequent features, B and C, are associated with the first and second multipath arrivals, respectively.

In this example case, the filtering is performed using the *lowpass* function in MATLAB® Signal Processing Toolbox™ which creates a linear-phase FIR lowpass filter with a 0.1 dB passband ripple [8]. The filter's linear phase is corrected for automatically by the filter

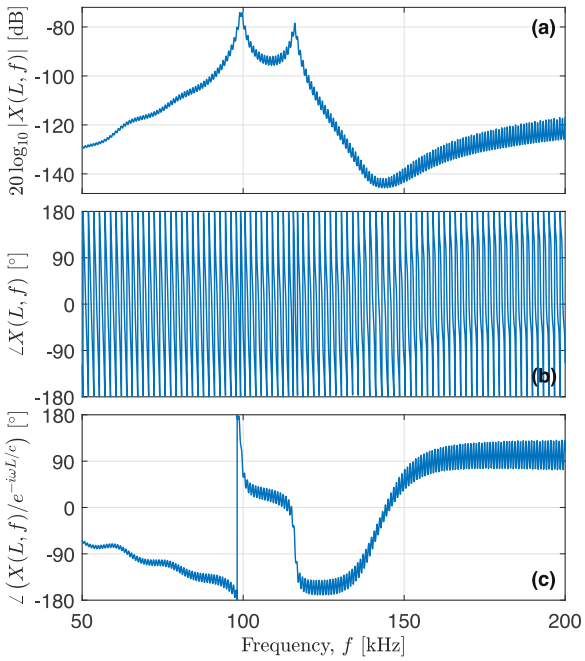

Fig. 2. Magnitude (a), phase angle (b), and slowly varying phase (c) of $X(L, f)$ for $L = 0.20$ m over the frequency range 50–200 kHz.

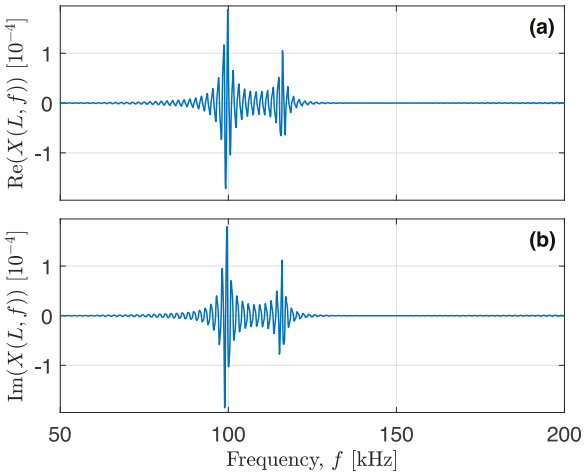

Fig. 3. Real (a) and imaginary (b) parts of $X(L, f)$ for $L = 0.20$ m over the frequency range 50–200 kHz.

function. For the filter used here, the passband extends from 0 to 1.64 ms. The passband is defined here as the band where the attenuation is within the passband ripple, i.e., –0.1 dB. A –60 dB stopband attenuation is used, and the stopband extends upwards from approximately 1.74 ms. The stopband is defined here as the band where the attenuation is at least –60 dB. The upper limit of the passband and lower limit of the stopband are shown as vertical dashed lines in Fig. 4. The real and imaginary parts of $X(L, f)$ and of the filtered $X(L, f)$, i.e. $X_1(L, f)$, are shown in Fig. 5, and the corresponding SoSs are shown in Fig. 6.

It can be seen from Fig. 4 that the tail of feature A, associated with the direct arrival, has a non-negligible magnitude at the onset of feature B, associated with the first multipath arrival. This indicates that the tail of feature A extends into feature B, and this part will thus be removed by the lowpass filtering since it is in the stopband of the filter. An additional part of this tail is removed due to the gradual roll-off of the filter between the passband and the stopband. These issues, together with the small passband ripple, mean that some information about the direct arrival is lost in the SoS filtering of the frequency spectrum when the tail of feature A extends beyond the passband of the lowpass filter. This effect may be reduced by application-specific preprocessing, as shown in a later section.

Step 4: The final step is here to recombine the filtered real and imaginary parts of $X(L, f)$, i.e., $\mathrm{Re}(X_1(L, f))$ and $\mathrm{Im}(X_1(L, f))$. Fig. 7 shows the input $X(L, f)$ containing both direct and multipatharrivals, and $X_1(L, f)$ primarily containing information about

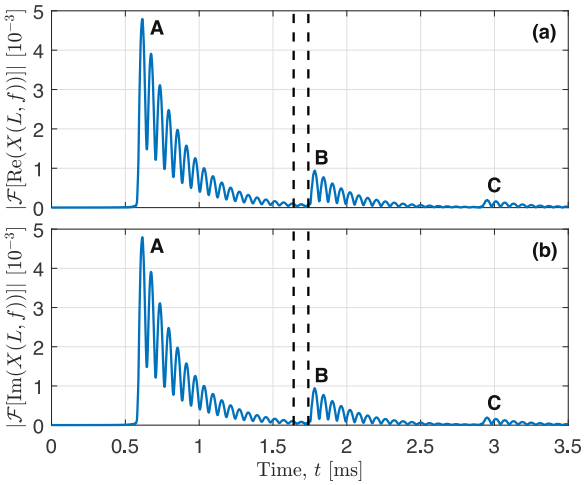

Fig. 4. Magnitude of the individual forward Fourier transforms of the real (a) and imaginary (b) parts of $X(L, f)$, i.e., the SoS of $X(L, f)$, for $L = 0.20$ m, over the frequency range 50–200 kHz. Due to symmetry only the one-sided SoS is shown, for times up to 3.5 ms. The labels A, B, and C indicate the onset of the features associated with the direct, first and second multipath arrivals. Vertical dashed lines indicate chosen passband and stopband limits of the SoS lowpass filter to be applied.

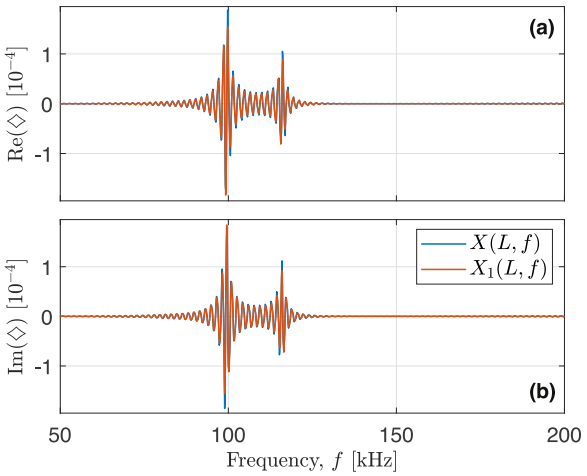

Fig. 5. Real (a) and imaginary (b) parts of $X(L, f)$ and $X_1(L, f)$ for $L = 0.20$ m over the frequency range 50–200 kHz.

the direct arrival. It is seen from the plots of the magnitude (a) and slowly varying phase angle (c) that the oscillations caused by multipath interference essentially are removed. This is also the case for the phase angle (b), but it is not as easily observed. The removal of some information related to the direct arrival in the filtering, as discussed under steps 2 and 3, leads to the presence of small oscillations with amplitudes of up to approximately 0.2 dB and 1.3° in $X_1(L, f)$. These oscillations are too small to be visible in Fig. 7. There are also undesired oscillations at either end of $X_1(L, f)$ in Fig. 7 due to truncation effects resembling the Gibbs effect. These can be reduced for instance by including a larger frequency range in the input to the SoS filtering and later omitting either end from the presented results. For the results Fig. 7, the truncation effects in $X_1(L, f)$ are negligible at approximately 55 kHz, i.e., 5 kHz from the lower end of the spectrum, and at approximately 188 kHz, i.e., 12 kHz from the upper end of the spectrum.

Example including application-specific preprocessing

For some cases, improved results can be obtained by using application-specific preprocessing of $X(L, f)$ prior to SoS filtering, and a corresponding postprocessing after SoS filtering. This is shown here for an example case identical to the one described above, but with $L = 0.10$ m as the distance between the transducers instead of $L = 0.20$ m. In contrast to the $L = 0.20$ m case, reduced distance to $L = 0.10$ m causes the rate of change of the rapid changes around the resonance peaks in $X(L, f)$ to be as large, or larger, than that of the oscillations caused by the multipath arrivals. This is mainly due to the changes in the oscillations cause by the multipath arrivals since the rate of change of the rapid changes around the resonance peaks in $X(L, f)$ is almost identical for the two distances.

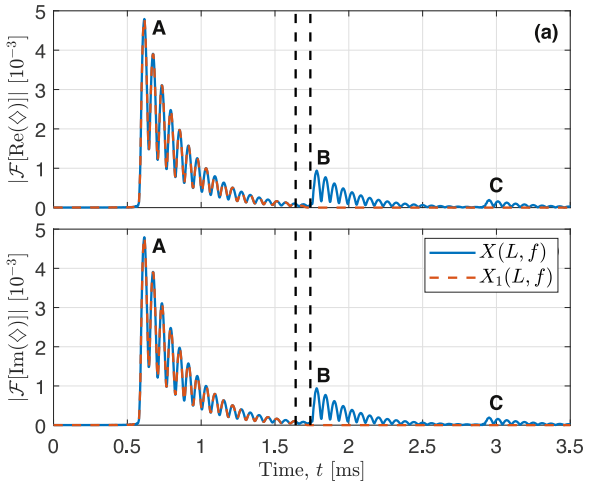

Fig. 6. Magnitude of the individual forward Fourier transforms of the real (a) and imaginary (b) parts of $X(L,f)$ and $X_1(L,f)$, i.e., the SoS of $X(L,f)$ and $X_1(L,f)$, for $L = 0.20$ m over the frequency range 50–200 kHz. The $X(L,f)$ results are the same as in Fig. 4, as are the filter settings indicated by the vertical dashed lines.

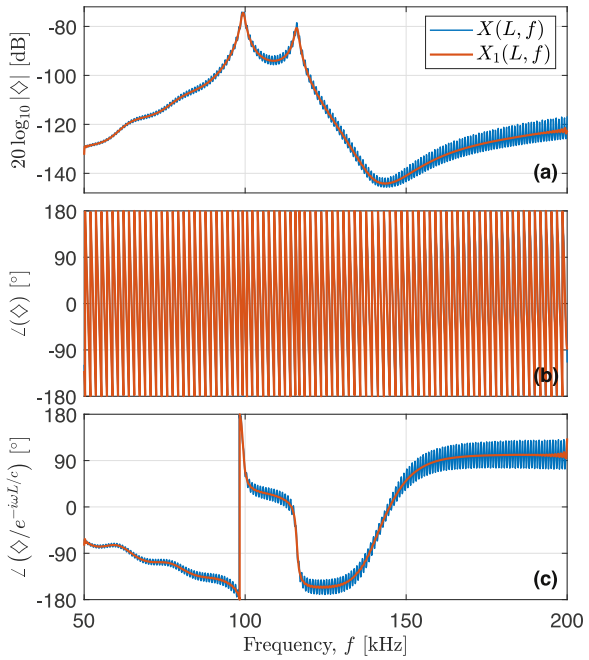

Fig. 7. Magnitude (a), phase angle (b), and slowly varying phase angle (c) of $X(L,f)$ and $X_1(L,f)$, for $L = 0.20$ m over the frequency range 50–200 kHz. The input $X(L,f)$ contains both direct and multipath arrivals, while $X_1(L,f)$ primarily contains information about the direct arrival.

However, the resonance peaks in $X(L,f)$ do not extend over the same time span in the SoS since it is closely linked to the onset of each feature, which in turn are associated with the different arrivals. This is for instance seen in Fig. 6 where there is no information prior to the onset of feature A. As a result, it is the time between the onset of the features A and B that determines whether the rate of change around the resonance peaks in $X(L,f)$ is as fast, or faster, than the oscillations caused by multipath interference. From Eq. (6) it can be calculated that this time span decreases from approximately 1.2 m/s to 0.6 ms when the distance decreases from $L = 0.20$ m to $L = 0.10$ m.

A comparison of the SoS of $X(L,f)$ for $L = 0.10$ m and $L = 0.20$ m, shown in Figs. 8 and 4, respectively, shows that the tail of feature A at the onset of feature B is larger for $L = 0.10$ m than for $L = 0.20$ m. This indicates that without preprocessing and subsequent postprocessing, SoS filtering of $X(L,f)$ would remove more of the information related to the direct arrival when $L = 0.10$ m than when $L = 0.20$ m.

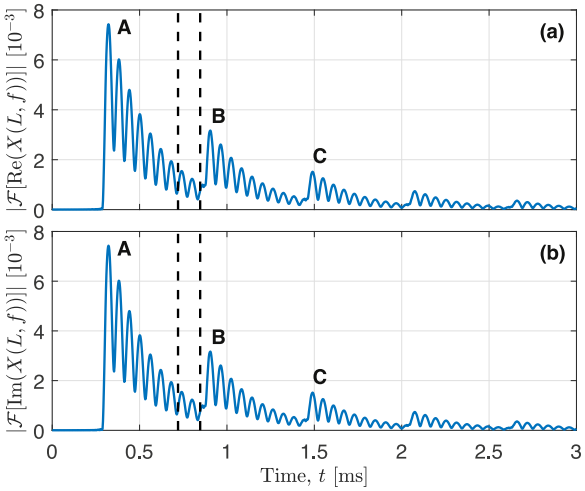

Fig. 8. Magnitude of the forward Fourier transforms of the real (a) and imaginary (b) parts of $X(L, f)$, i.e., the SoS of $X(L, f)$, for $L = 0.10$ m over the frequency range 50–200 kHz. The vertical dashed lines indicate the upper limit of the passband, 0.72 ms, and the lower limit of the stopband, approximately 0.85 ms.

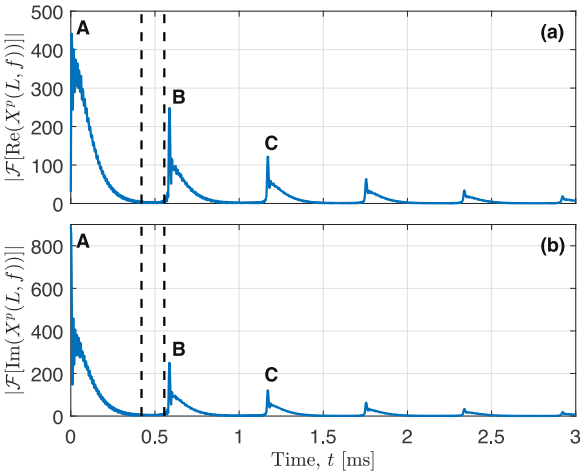

Fig. 9. Magnitude of the forward Fourier transforms of the real (a) and imaginary (b) parts of $X^p(L, f)$, i.e., the SoS of $X^p(L, f)$, for $L = 0.10$ m over the frequency range 50–200 kHz. The vertical dashed lines indicate the upper limit of the passband, 0.42 ms, and the lower limit of the stopband, approximately 0.56 ms.

To reduce such undesired effects, the application-specific preprocessing used for $L = 0.10$ m is

$$X^p(L, f) = H^{VV}(L, f)/H^{VV}_{ff,e}(L, f, n = 1), \tag{7}$$

where $H^{VV}_{ff,e}(L, f, n)$ is a simplified far-field transfer function extrapolated spherically back to a distance $(2n - 1)L$ for the nth arrival, defined as

$$H^{VV}_{ff,e}(L, f, n) = \left(\frac{p(z_{ff}, f)}{V_{in}(f)}\right)^2 Z(f)\frac{z_{ff}^2}{(2n-1)L} e^{i\frac{\omega}{c}2z_{ff}} e^{-i\omega(2n-1)L/c}\,. \tag{8}$$

Here, $p(z_{ff}, f)$ is the axial free-field pressure at the far-field distance z_{ff} generated by the transmitting piezoelectric disk with electrical input impedance $Z(f)$ when excited by the voltage $V_{in}(f)$. See Sec. 2.4 in [2] for details. $p(z_{ff}, f)$ and $Z(f)$ are calculated by a 3D axisymmetric transmitter-medium FE model [10], different from the transmitter-medium-receiver FE model used to calculate $H^{VV}(L, f)$. $H^{VV}_{ff,e}(L, f, n = 1)$ contains the sharp resonance peaks in the frequency spectrum, but neither nearfield effects, diffraction effects for a non-plane incident wave, nor reflection from a finite object (transducer).

Fig. 9 shows the SoS of $X^p(L, f)$ and it is seen that the tails following the distinct features decrease much faster here than for $X(L, f)$ in Fig. 8, indicating that $X^p(L, f)$ contains less rapid changes than $X(L, f)$. The vertical dashed lines in Figs. 8 and 9 indicate the upper limit of the passband and lower limit of the stopband for the lowpass FIR filter used to extract the direct arrival for $L = 0.10$

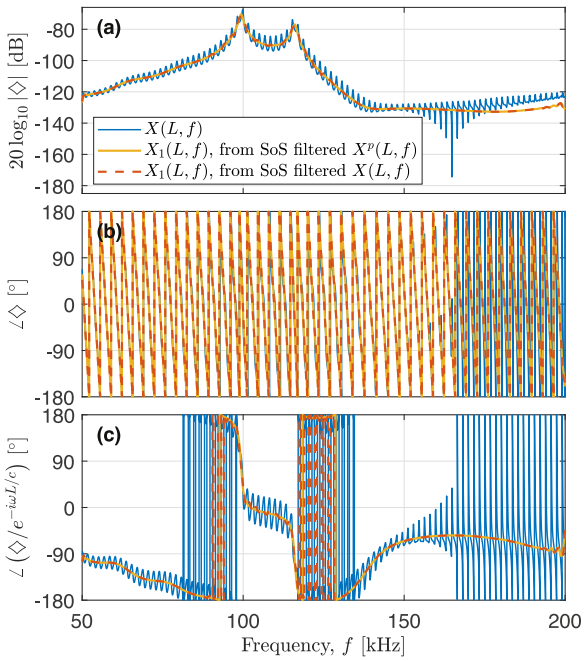

Fig. 10. Magnitude (a), phase angle (b), and slowly varying phase angle (c) of $X(L,f)$ and $X_1(L,f)$, for $L = 0.10$ m over the frequency range 50–200 kHz. The input $X(L,f)$ contains both direct and multipath arrivals, while $X_1(L,f)$ primarily contains information about the direct arrival. Two results for $X_1(L,f)$ are shown, obtained using SoS filtering of $X(L,f)$ and $X^p(L,f)$, respectively.

m, i.e., 0.72 and 0.85 ms for $X(L,f)$ and 0.4 ms and 0.56 ms for $X^p(L,f)$, respectively. These are different in the two figures since the preprocessing moves the onset of feature A from approximately 2.9 ms in Fig. 8 to the origin in Fig. 9, and also move the other features correspondingly.

Fig. 10 shows the input $X(L,f)$ and the extracted $X_1(L,f)$ obtained with and without preprocessing, i.e., by SoS filtering of $X^p(L,f)$ and $X(L,f)$, respectively, for $L = 0.10$ m over the frequency band 50–200 kHz. The same results are shown in Fig. 11, but over the frequency band around the resonances, 85–130 kHz. From these two figures it is seen that the two methods perform equally well outside the frequency band of the resonances. SoS filtering of $X^p(L,f)$ yields good results also in the frequency band around the resonances, while the results obtained from SoS filtering of $X(L,f)$ have undesired oscillations in the 85–130 kHz frequency band.

Note that the large oscillations in the slowly varying phase of $X(L,f)$ and $X_1(L,f)$ (obtained from the SoS filtering of $X(L,f)$) in the two frequency bands 80–100 kHz and 115–135 kHz are not caused by a physical effect, but by relatively small oscillations close to 180° and –180° and thus subject to phase wrapping multiple times [7]. The deviation between the filtered and unfiltered results for the magnitude at frequencies above approximately 170 kHz, is not an error, but rather an indication that one or several of the multipath arrivals are stronger than the direct arrival [7].

Theoretical plane wave example

A theoretical example of how the SoS filtering method can be used to extract the direct arrival and the first multipath arrival is given here. A simplified plane wave example is presented, with one direct and two multipath arrivals with amplitudes, A_n, that are constant with respect to frequency. In the frequency domain, with the time dependence $e^{i\omega t}$ suppressed, the plane wave pressure for the direct arrival is given as

$$p_1(L,f) = A_1 e^{-i\omega\frac{L}{c}}. \tag{9}$$

Similarly, the first and second multipath arrivals are, when assuming reflection at each interface as from a rigid infinite plate, given as

$$p_2(L,f) = A_2 e^{-i\omega\frac{3L}{c}}, \tag{10}$$

and

$$p_3(L,f) = A_3 e^{-i\omega\frac{5L}{c}}, \tag{11}$$

respectively. A_1, A_2, and A_3 are the amplitudes of the three arrivals, respectively. The total pressure is the sum of the three arrivals, i.e.,

$$p_{tot}(L,f) = p_1(L,f) + p_2(L,f) + p_3(L,f) = A_1 e^{-i\omega\frac{L}{c}} + A_2 e^{-i\omega\frac{3L}{c}} + A_3 e^{-i\omega\frac{5L}{c}}. \tag{12}$$

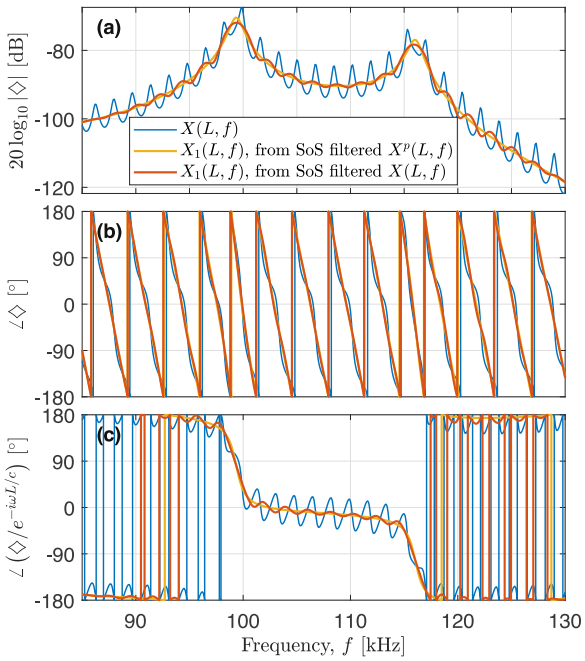

Fig. 11. Magnitude (a), phase angle (b), and slowly varying phase angle (c) of $X(L,f)$ and $X_1(L,f)$, for $L = 0.10$ m over the frequency range 85–130 kHz. The same results as in Fig. 10, but shown for a smaller frequency range.

Dividing Eq. (12) with the plane wave phase term for the direct arrival yields

$$p_{tot}(L,f)/e^{-i\omega\frac{L}{c}} = A_1 + A_2 e^{-i\omega\frac{2L}{c}} + A_3 e^{-i\omega\frac{4L}{c}}, \tag{13}$$

which then can be split into its real part,

$$\mathrm{Re}\left\{ p_{tot}(L,f)/e^{-i\omega\frac{L}{c}} \right\} = A_1 + A_2\cos\left(\omega\frac{2L}{c}\right) + A_3\cos\left(\omega\frac{4L}{c}\right), \tag{14}$$

and its imaginary part,

$$\mathrm{Im}\left\{ p_{tot}(L,f)/e^{-i\omega\frac{L}{c}} \right\} = -\left[A_2\sin\left(\omega\frac{2L}{c}\right) + A_3\sin\left(\omega\frac{4L}{c}\right)\right]. \tag{15}$$

The last two terms on the right-hand side of Eq. (14) and the two terms on the right-hand side of Eq. (15) are the oscillating terms associated with the multipath arrivals. Individual lowpass filtering of Eqs. (14) and (15) using a stopband that includes oscillations from $2L/c$ and upwards will remove these terms, yielding the filtered real part,

$$\overline{\mathrm{Re}\left\{ p_{tot}(L,f)/e^{-i\omega\frac{L}{c}} \right\}} \simeq A_1, \tag{16}$$

and the filtered imaginary part,

$$\overline{\mathrm{Im}\left\{ p_{tot}(L,f)/e^{-i\omega\frac{L}{c}} \right\}} \simeq 0, \tag{17}$$

where the overbar indicates lowpass filtering. Recombining the lowpass filtered real and imaginary parts and multiplying with the plane wave phase term for the direct arrival yields

$$\overline{p_{tot}(L,f)} = \left[\overline{\mathrm{Re}\left\{ \frac{p_{tot}(L,f)}{e^{-i\omega\frac{L}{c}}} \right\}} + i\,\overline{\mathrm{Im}\left\{ \frac{p_{tot}(L,f)}{e^{-i\omega\frac{L}{c}}} \right\}} \right] e^{-i\omega\frac{L}{c}} \simeq A_1 e^{-i\omega\frac{L}{c}} = p_1(L,f). \tag{18}$$

This shows that the SoS lowpass filtering method gives exact extraction of the direct arrival's spectrum for this simplified plane wave case. To extract the first multipath arrival's spectrum, the result from Eq. (18) is subtracted from Eq. (12) to give

$$p_{2+}(L,f) \simeq p_{tot}(L,f) - p_1(L,f) = A_2 e^{-i\omega 3L/c} + A_3 e^{-i\omega 5L/c}, \tag{19}$$

where the subscript "2+" indicates that it is the sum of the first and second multipath arrivals. Dividing Eq. (19) by the plane wave phase term for the first multipath arrival yields

$$p_{2+}(L,f)/e^{-\omega 3L/c} \simeq A_2 + A_3 e^{-i\omega 2L/c}, \tag{20}$$

```
%% Example code for the SoS filtering method using plane waves

% The essential part is the SoS filtering, implemented by:
% Xp_filt = lowpass(Xp,passband_limit,1/f_step,'Steepness',filter_steepness,...
%       'ImpulseResponse','fir','StopbandAttenuation',60);

%% Problem description
c = 343;                        % [m/s] Sound velocity in air
L = 0.10;                       % [m] Distance between transducers
f_step = 100;                   % [Hz] Frequency step in spectrum
f = 0:f_step:200e3;             % [Hz] Frequency spectrum
omega = 2*pi*f;                 % [rad/s] Angular frequency

A1 = 1;                         % Amplitude of direct arrival
A2 = 0.8;                       % Amplitude of first multipath arrival
A3 = 0.4;                       % Amplitude of second multipath arrival

% Settings SoS calculation
N = 2^12;                       % Points in the fft
Ts = 1/f_step;                  % Sampling time
t_step = Ts/N;                  % Time step in the SoS results
t = 0:t_step:(Ts/2-t_step);     % Time vector for SoS results

%% SoS filtering steps to obtain the direct arrival

% Step 1: Input frequency spectrum
X = A1*exp(-1i*omega*L/c) + A2*exp(-1i*omega*3*L/c) + A3*exp(-1i*omega*5*L/c);

% Optional step: Preprocessing of input frequency spectrum, e.g.,
Xp = X./exp(-1i*omega*L/c);

% Step 2: Calculate SoS to determine filter settings
real_SoS = fft(real(Xp),N); imag_SoS = fft(imag(Xp),N);

% Plot SoS
figure(1), plot(t,abs(real_SoS(1:N/2))), hold all, plot(t,abs(imag_SoS(1:N/2)))
xlabel('Time [s]'), ylabel('|FFT(-)|'), legend('|FFT[Re(X_p)]|','|FFT[Im(X_p)]|')

% Initial filter settings determined from visual inspection of plots
passband_limit = 3e-4; filter_steepness = 0.96;

% Test initial filtering. If stopband does not include desired features,
% adjust filter settings and try again until OK.
[~, params] = lowpass(Xp,passband_limit,Ts,'Steepness',filter_steepness,...
    'ImpulseResponse','fir','StopbandAttenuation',60);
disp(['Stopband lower limit: ' num2str(params.StopbandFrequency) ' s'])
plot([1 1]*params.StopbandFrequency,ylim,'k--')

% Step 3 & 4: Apply FIR filter to real and imaginary parts and recombine
Xp_filt = lowpass(Xp,passband_limit,Ts,'Steepness',filter_steepness,...
    'ImpulseResponse','fir','StopbandAttenuation',60);

% If preprocessing: Calculate filtered X from filtered Xp
X_filt = Xp_filt.*exp(-1i*omega*L/c);

% Plot results
figure, plot(f,abs(X)), hold all, plot(f,abs(X_filt),'LineWidth',1.5)
plot([f(1) f(end)],[A1 A1],'--','LineWidth',1.5), xlabel('Frequency [Hz]')
ylabel('Magnitude'), legend('X: Input frequency spectrum',...
    'X_{filt}: SoS filtered X','A1: Reference')
```

Fig. 12. MATLAB® code implementing SoS filtering of the frequency spectrum to extract the direct arrival, for the simplified plane wave example described above.

```
%% SoS filtering to obtain first multipath arrival

% Step 1: Subtract result for direct arrival
X2 = X - X_filt;

% Optional step: Preprocessing
X2p = X2./exp(-1i*omega*3*L/c);

% Step 2: Calculate SoS to determine filter settings
real_SoS2 = fft(real(X2p),N); imag_SoS2 = fft(imag(X2p),N);

% Plot SoS
figure(3), plot(t,abs(real_SoS2(1:N/2))), hold all, plot(t,abs(imag_SoS2(1:N/2)))
xlabel('Time [s]'), ylabel('|FFT(-)|'), legend('|FFT[Re(X2_p)]|','|FFT[Im(X2_p)]|')

% The preprocessing enables the use of the same filter settings as before
passband_limit = 3e-4; filter_steepness = 0.96;

% Step 3 & 4: Apply FIR filter to real and imaginary parts and recombine
X2p_filt = lowpass(X2p,passband_limit,Ts,'Steepness',filter_steepness,...
    'ImpulseResponse','fir','StopbandAttenuation',60);

% If preprocessing: Calculate filtered X2 from filtered X2p
X2_filt = X2p_filt.*exp(-1i*omega*3*L/c);

% Plot results
figure(4), hold all, plot(f,abs(X2)), plot(f,abs(X2_filt),'LineWidth',1.5)
plot([f(1) f(end)],[A2 A2],'--','LineWidth',1.5), xlabel('Frequency [Hz]')
ylabel('Magnitude'), legend('X2: Input frequency spectrum',...
    'X2_{filt}: SoS filtered X2','A2: Reference')
```

Fig. 13. MATLAB® code implementing SoS filtering of the frequency spectrum to extract the first multipath arrival, for the simplified plane wave example described above. It is to be appended to the code in Fig. 12.

which when separated into its real and imaginary parts, and lowpass filtered with a stopband that includes oscillations from $2L/c$ and upwards, yields

$$\overline{\mathrm{Re}\left\{ p_{2+}(L,f)/e^{-i\omega\frac{3L}{c}} \right\}} \simeq \overline{A_2 + A_3 \cos\left(\omega\frac{2L}{c}\right)} \simeq A_2, \tag{21}$$

and

$$\overline{\mathrm{Im}\left\{ p_{2+}(L,f)/e^{-i\omega\frac{3L}{c}} \right\}} \simeq \overline{A_3 \sin\left(\omega\frac{2L}{c}\right)} \simeq 0. \tag{22}$$

Recombining Eqs. (21) and (22) and multiplying them with the plane wave phase term for the first multipath arrival yields

$$\overline{p_{2+}(L,f)} = \left[\overline{\mathrm{Re}\left\{ \frac{p_{2+}(L,f)}{e^{-i\omega\frac{3L}{c}}} \right\}} + i\,\overline{\mathrm{Im}\left\{ \frac{p_{2+}(L,f)}{e^{-i\omega\frac{3L}{c}}} \right\}} \right] e^{-i\omega\frac{3L}{c}} \cong A_2 e^{-i\omega\frac{3L}{c}} = p_2(L,f), \tag{23}$$

showing that the SoS filtering of the frequency spectrum gives exact extraction of the first multipath arrival's spectrum in this simplified plane wave case.

Funding

This work was supported by the Research Council of Norway (RCN) under grant number 303169. RCN had no involvement in design or execution of the study, or in the writing of this article.

Declaration of Competing Interest

The authors declare that they have no known competing financial interests or personal relationships that could have appeared to influence the work reported in this paper.

CRediT authorship contribution statement

Eivind Nag Mosland: Conceptualization, Methodology, Software, Validation, Writing – original draft. **Per Lunde:** Writing – review & editing, Supervision, Project administration, Funding acquisition. **Jan Kocbach:** Writing – review & editing, Supervision, Funding acquisition.

Data availability

Data will be made available on request.

Acknowledgments

The authors want to thank Magne Vestrheim, University of Bergen, Norway, for discussions and feedback during this work.

References

[1] O. Brigham, in: The fast Fourier transform and its applications, Prentice-Hall, Inc., Englewood Cliffs, NJ, 1988, pp. 341–344.
[2] E. Storheim, Diffraction effects in the ultrasonic field of transmitting and receiving circular piezoceramic disks in radial mode vibration, Department of Physics and Technology, University of Bergen, Bergen, Norway, 2015 Ph.D. dissertation.
[3] R.B. Randall, A history of cepstrum analysis and its application to mechanical problems, Mech. Syst. Signal Process. 97 (2017) 3–19.
[4] C. Bao, J.R. Jimenez, S. Gelinsky, R. van der Weiden, Seismic resonance: wavelet-free reflectivity retrieval via modified cepstral decomposition, Geophysics 87 (1) (2021) IM11–IM24.
[5] M. Hall, Predicting bed thickness with cepstral decomposition, Lead. Edge 25 (2) (2006) 199–204.
[6] T.J. Cohen, Source-depth determinations using spectral, pseudo-autocorrelation and cepstral analysis, Geophys. J. Int. 20 (2) (1970) 223–231.
[7] E.N. Mosland, P. Lunde, J. Kocbach, Using spectrum-of-spectrum (SoS) filtering to extract direct and multipath arrivals from a frequency domain simulation. Comparison with cepstrum and time-gating methods, in: Proceedings of the 46th Scandinavian Symposium on Physical Acoustics, Geilo, Norway, 2023 January 30 - February 1.
[8] MathWorks Inc. “Lowpass command, MATLAB® R2021a,” December 22nd, 2022; https://se.mathworks.com/help/releases/R2021a/signal/ref/lowpass.html.
[9] E.N. Mosland, P. Lunde, J. Kocbach, Finite element-based diffraction correction for piezoelectric transducers accounting for diffraction at transmission, propagation, and reception, J. Acoust. Soc. Am. 154 (2023) 2177–2190.
[10] E.N. Mosland, J. Kocbach, E. Storheim, P. Lunde, Radiation in air from a piezoelectric ceramic disk in radial mode vibration. Contributions from front, side and rear surfaces, in: Proceedings of the 45th Scandinavian Symposium on Physical Acoustics, 2022 Online, January 31 - February 1.